Broadband Emission in Two-Dimensional Hybrid Perovskites: The Role of Structural Deformation

Cortecchia, Daniele; Neutzner, Stefanie; Srimath Kandada, Ajay Ram; Mosconi, Edoardo; Meggiolaro, Daniele; De Angelis, Filippo; Soci, Cesare; Petrozza, Annamaria

2016

Cortecchia, D., Neutzner, S., Srimath Kandada, A. R., Mosconi, E., Meggiolaro, D., De Angelis, F., et al. (2017). Broadband Emission in Two-Dimensional Hybrid Perovskites: The Role of Structural Deformation. Journal of the American Chemical Society, 139(1), 39-42.

https://hdl.handle.net/10356/86312

https://doi.org/10.1021/jacs.6b10390

Broadband Emission in Two-dimensional Hybrid Perovskites: the Role of Structural Deformation

Daniele Cortecchia[1,2], Stefanie Neutzner[2], Ajay Ram Srimath Kandada[2], Edoardo Mosconi[3,4], Daniele Meggiolaro[3,4], Filippo De Angelis[3,4*], Cesare Soci[5] and Annamaria Petrozza[2*]

1 Interdisciplinary Graduate School, Energy Research Institute @ NTU(ERI@N), Nanyang Technological University, Singapore 639798, Singapore.
2 Istituto Italiano de Tecnologia, Centre for Nano Science and Technology (CNST@PoliMi), Milan, 20133, Italy
3 Istituto CNR di Scienze e Tecnologie Molecolari, c/o Dipartimento di Chimica, Università di Perugia, Perugia, I-06123, Italy
4 CompuNet, Istituto Italiano di Tecnologia, Via Morego 30, 16163 Genova, Italy
5 Division of Physics and Applied Physics, School of Physical and Mathematical Sciences, Nanyang Technological University, Singapore 637371, Singapore.

ABSTRACT: Only a selected group of two-dimensional (2D) lead-halide perovskites shows a peculiar broad-band photoluminescence, arising from self-localized charges, in contrast to the typical free-excitonic emission. Here we show that the structural distortions of the perovskite lattice can determine the defectivity of the material by modulating the defect formation energies. By selecting and comparing two archetype systems, namely $(NBT)_2PbI_4$ and $(EDBE)PbI_4$ perovskites (NBT=n-butylammonium and EDBE=2,2-(ethylenedioxy)-bis(ethylammonium), we find that only the latter, subject to larger deformation of the Pb-X bond length and X-Pb-X bond angles, sees the formation of V_F color centers, whose radiative decay ultimately leads to broadened PL. These findings highlight the importance of structural engineering to control the optoelectronic properties of this class of soft materials.

Hybrid perovskites provide the unique opportunity of tuning the dimensionality of the electronic landscape by controlling the nature of the organic cation.[1] 3D perovskites have been successfully employed in photovoltaic and light emitting devices[2,3] and 2D perovskites have recently been explored.[4-6] These consist of alternating organic and inorganic layers, with charge carriers confined within the inorganic network, similar to a multi-quantum well structure. This leads to a large exciton binding energy (EBE) up to 300 meV,[1] compared to 3D perovskites where EBE is less than 50 meV.[7] Therefore, 2D perovskites usually show extremely narrow-band photoluminescence (PL) spectra, typically belonging to free-excitonic states, holding a great promise in advanced optoelectronics.[8,9] A subclass of 2D perovskites however has recently attracted attention for their potential application in broadband solid-state lighting for the presence of highly Stokes-shifted light emission with full width at half maximum (FWHM) up to 600-700 meV.[10]

Such broadband emission was observed irrespective of the crystal orientation and with no evident correlation to the chemical composition.[10-13] Recently, its appearance in Cl and Br based perovskites was ascribed to charge self-trapping phenomena.[14-16] However, the reason why self-localization is favored only in certain perovskites, in competition with sharp free-excitonic emission, is yet to be clarified. Structural deformations in traditional inorganic perovskites are known to play fundamental roles in ferro- and piezo-electricity and superconductivity.[17] Despite molecular rotations and octahedral distortions were considered in theoretical works on 3D perovskites,[18] their influence on luminescence properties has not yet been investigated. Here, we show that structural distortions of the inorganic lattice play a key role in carrier localization and the subsequent broadband emission.

Synthetic chemistry offers powerful tools to control the perovskite structural properties. Here we synthetize, *ad hoc*, two representative 2D perovskites, $(NBT)_2PbI_4$ and $(EDBE)PbI_4$ (Figure 1a,b), having the same inorganic network (PbI_4^{2-}), but assembling in distinct crystalline configurations. This is achieved by exploiting the templating mono- and ditopic organic cations NBT=n-butylammonium and EDBE=2,2-(ethylenedioxy)bis(ethylammonium) (Figure 1a,b). These two linkers direct the crystal growth along different perovskite cuts, resulting in the flat <100>-oriented $(NBT)_2PbI_4$ and rippled $(EDBE)PbI_4$, characterized by the <110>-oriented zig-zag structure.[10,19] These were reported to crystallize with orthorhombic and monoclinic crystal system respectively,[10,19] in agreement with our thin film X-ray diffraction measurements (Figure S1).

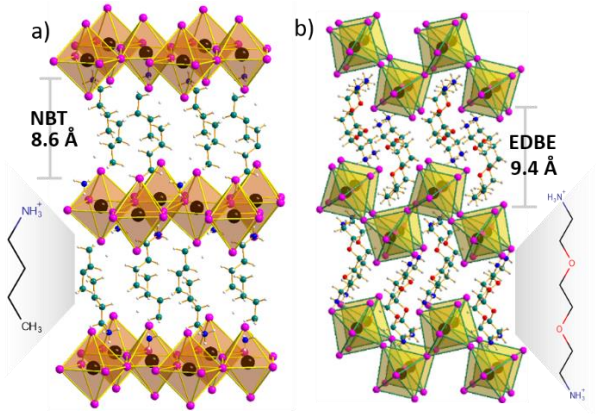

Figure 1. Crystal structures of a) $(NBT)_2PbI_4$[19] and b) $(EDBE)PbI_4$,[10] with their templating cations: NBT=n-butylammonium and EDBE=2,2-(ethylenedioxy)bis(ethylammonium).

To investigate the effect of such structural difference, we performed Raman measurements on perovskite crystals (Figure 2), films (Figure S2) and iodide salts of their organic precursors. Similarly to the Raman spectrum of $MAPbI_3$ (MA=methylammonium), four bands appear between 80-300 cm^{-1} (Figures 2a,b).[20] Following previous assignments,[20-23] we attribute the band at 99 cm^{-1} to the Pb-I stretching mode. The remaining three bands are assigned to vibrational modes of the ammonium moieties coupled with the inorganic part. The signals at 116-118 cm^{-1} and 136 cm^{-1} are ascribed to libration modes, and the band at 183 cm^{-1} to torsional modes.[20,22] While the peak at 99 cm^{-1} is prominent in the Raman spectrum of $(NBT)_2PbI_4$, resembling that of $MAPbI_3$, it is partially deactivated in $(EDBE)PbI_4$; such weakening of the Pb-I intensity mode results from the increased angular distortion of the latter (Table S1 and S2). Moreover, the band at 183 cm^{-1} is silent in $(EDBE)PbI_4$ and the strength of the 136 cm^{-1} mode is significantly reduced. This observation can be interpreted as a higher degree of conformational constraint of the ammonium moieties in the <110>-oriented perovskite, strongly interacting with the enclosing inorganic lattice.[24]

We also compare the Raman spectra of the organic cation (between 300-1500cm^{-1}) within the perovskite lattice and the pristine molecules (Figure 2c,d). Here, the spectral features belong to pure vibrational modes of the organic part.[21,25] (NBT)I preserves all its active modes when embedded in the perovskite with only small changes in the relative intensities of the peaks (Figure 2c). On the contrary, new modes appear in $(EDBE)I_2$ when co-crystallized with PbI_2 (black arrows in Figure 2d). We argue that $EDBE^{2+}$ in the perovskite is forced into a different conformation due to its greater interaction with the inorganic cage, mutually affecting the distortion of the Pb-I framework.

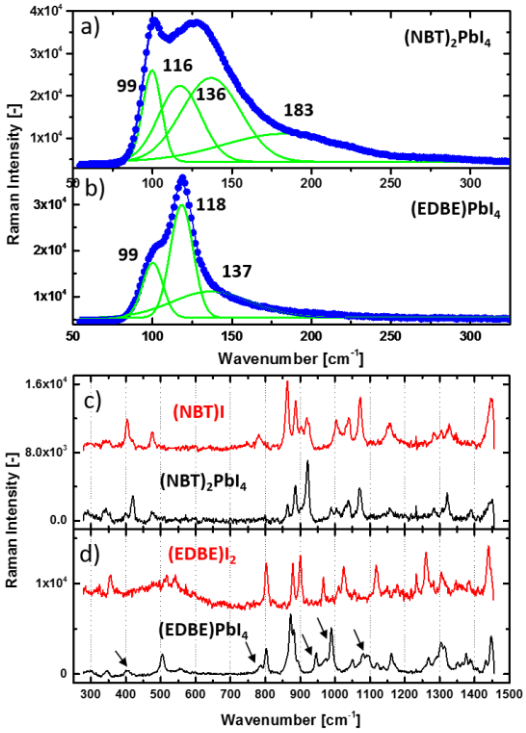

Figure 2. Raman spectra of a,c) $(NBT)_2PbI_4$ and b,d) $(EDBE)PbI_4$. c,d) active modes of the pure iodide salts (red) and those of the organic cation after formation of the perovskite (black). The black arrows indicate new active modes of $EDBE^{2+}$ upon perovskite formation.

The consequences of such structural transformation on the optical properties are important. The absorption and PL spectra of polycrystalline films (Figure S3) are shown in Figures 3a,b. The optical band-edge of $(EDBE)PbI_4$ is blue shifted by 44 nm with respect to $(NBT)_2PbI_4$ with excitonic resonances at 469 nm and 513 nm, respectively (Figure 3). This drastic change in band-gap is a fingerprint of the different structural arrangement of the inorganic framework in the <100> and <110>-oriented perovskites.

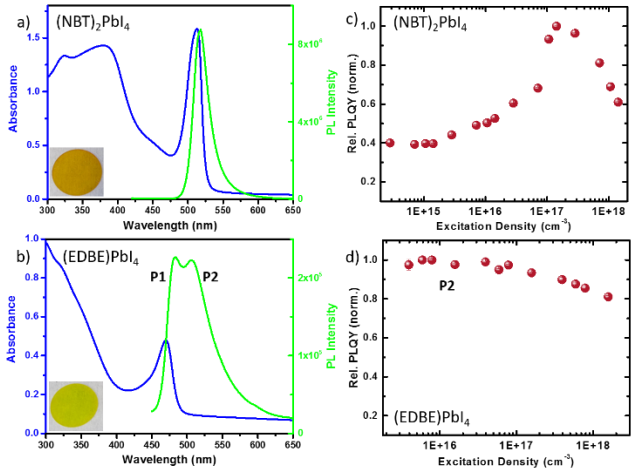

Figure 3. Steady state absorption (blue) and photoluminescence (green) of a) $(NBT)_2PbI_4$ and b) $(EDBE)PbI_4$. The insets show the structural induced color change (from orange to yellow). Relative photoluminescence quantum yield (PLQY) against excitation density for c) $(NBT)_2PbI_4$ and d) $(EDBE)PbI_4$.

$(NBT)_2PbI_4$ shows narrow-band emission (FWHM=25 nm) at 517 nm with Stokes shift of just 4 nm, while $(EDBE)PbI_4$ exhibits much broader PL (FWHM=70 nm) comprising of narrow-band bandgap emission peaked at 483 nm (P1), overlapped with a broader, red-shifted band at 507 nm (P2). P1 and P2 can be distinguished in thinner films, while thicker ones predominantly show a featureless broadband attributable to losses due to re-absorption (Figure S4). Both the materials have absolute photoluminescence quantum yield (PLQY) below 1%, with $(NBT)_2PbI_4$ being more emissive than $(EDBE)PbI_4$. To obtain reliable intensity dependent trends, it was essential to perform measurements on thicker samples, where it is not possible to clearly observe P1 in $(EDBE)PbI_4$ (Figure S4). Thus, the trend of only P2 is reported in Figure 3. In $(NBT)_2PbI_4$, the relative PLQY of the band-to-band emission enhances with excitation density, with a drop at high excitations due to Auger recombination (Figure 3c and S5). On the contrary, P2 in $(EDBE)PbI_4$ shows a monotonic reduction, suggesting its origin from electronic states whose occupation probability reduces at higher excitation densities (Figure 3d and Figure S5). An identical trend was observed in single crystals (Figure S6). Such behavior is reminiscent of PL from intra-gap defect states, saturated at higher densities. Presence of radiative defects within the perovskite lattice was also reported in 3D perovskites.[26-29] This implies that $(EDBE)PbI_4$ contains a higher density of radiative color centers.

To ascertain the structure-PL properties relationship, we determined the degree of structural strain of the perovskite considering the distortions of the inorganic building blocks, the octahedra PbX_6. The deformation of O_h symmetry involves modifications in Pb-X bond length (d) and X-Pb-X angles (α), with changes in edges length (X-X distances) and O_h volume (V) compared to the ideal structure.[30] Robinson *et al*[31] developed a quantitative evaluation of these parameters introducing the octahedral elongation λ_{oct} and octahedral angle variance σ^2_{oct}:

$$\lambda_{oct} = \frac{1}{6}\sum_{i=1}^{6}(d_i/d_0)^2 \qquad [1]$$

$$\sigma^2_{oct} = \frac{1}{11}\sum_{i=1}^{12}(\alpha_i - 90)^2 \qquad [2]$$

where d_i are the Pb-X bond lengths, d_o is the center-to-vertex distance of a regular polyhedron of the same volume and α_i are the X-Pb-X angles. PL broadening follows the increased structural distortion of $(EDBE)PbI_4$ (λ_{oct}=1.0058; σ^2_{oct}=14.2) compared to $(NBT)_2PbI_4$ (λ_{oct}=1.0016; σ^2_{oct}=5.6). This observation is corroborated by evaluating the structural parameters of broadband emitting perovskites compared to those of typical narrowband emitters (Table S1 and S2). By plotting λ_{oct} against σ^2_{oct} it appears that higher distortion factors closely correlate with PL broadening (Figure S7).

To rationalize the structural effects on the defectivity and energetic landscape, we performed ab-initio calculations on perfect and defective crystals, considering iodine interstitials and vacancies (I_i, V_I), and lead vacancies (V_{Pb}) (Figure S8 and Table S3).[32] We find two different structures for the neutral Pb vacancy: i) a relaxed structure where a vicinal iodine moves to the V_{Pb} site to form an I_3^- trimer (Figure 4a); and ii) a structure with V_{Pb} remaining in the position where the lead was removed (Figure 4b), similar to the stable structure found for the 2- and 1- charge states.[33,34] The stability of the two structures depends on the material: while these are isoenergetic in $(NBT)PbI_4$, I_3^- formation is strongly favoured in $(EDBE)PbI_4$ by ~1 eV. The relaxed structure corresponds to the oxidation of two iodides by two holes left in the defect site upon neutral V_{Pb} formation. In $(EDBE)PbI_4$, the formation of the I_3^- is driven by under-coordinated iodine atoms at the organic/inorganic interface, only partly charge stabilized by $EDBE^{2+}$ and can thus lead to large lattice rearrangements. In $(NBT)_2PbI_4$, there is one frontier iodine atom per organic cation (two such iodine atoms are instead present in $(EDBE)PbI_4$) with consequently stronger electrostatic interaction that disfavors the vicinal iodine motion from forming I_3^-. Similar point defects, consisting in a V-center coupled to an adjacent cation vacancy, were demonstrated in LiF: these are known as V_F centers and regarded as "the antimorph of the F centers", involving the complementary electron trapping at a halogen vacancy.[35,36]

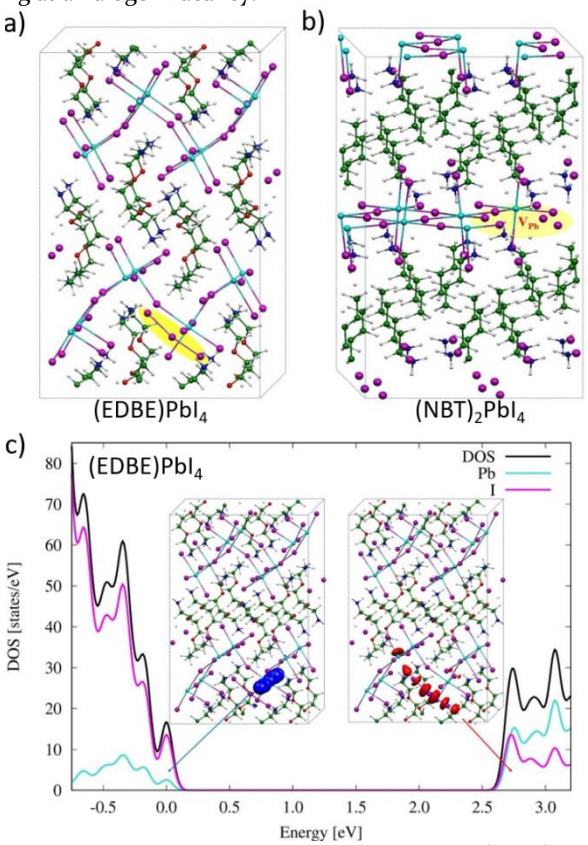

Figure 4. Geometry structures of neutral vacancy of $(EDBE)PbI_4$ (a) and $(NBT)_2PbI_4$ (b). DOS of the neutral lead vacancy $(EDBE)PbI_4$ (c) and the relative isodensity plot of the defect states.

Quantitative estimation of the electronic structure was achieved with hybrid DFT calculations including spin-orbit coupling (PBEo-SOC).[34] For the pristine $(EDBE)PbI_4$ we calculate a band-gap of 2.83 eV, excellently matching the experimental excitonic peak (2.64 eV), considering the typical EBE of 2D perovskites (200-300 meV). The introduction of neutral V_{Pb} generates two electronic states in the DOS (one occupied, one unoccupied) at 0.16 and 0.05 eV above and below the valence and conduction band edges (Figure 4c). The calculated optical absorption spectrum of the defective system, using the Random Phase Approximation neglecting non-local fields effects (Figure S9), highlights the presence of an optical transition at 2.92 eV, 0.21 eV below the main band-gap absorption peak. This corresponds to the HOMO-LUMO transition of I_3^-, with intensity of ~1/4 the cross section of the band gap transition. Therefore we associate the emergence of

these states with the emissive traps leading to Stokes-shifted, broadened luminescence according to the relaxation mechanism typical of trapped charge carriers.[13,14] Our analysis highlights the crucial role of the templating cation to assist charge localization, indicating that increased structural distortions in the PbX_6 octahedral coordination of (EDBE)PbI_4 lower the energy barrier for hole self-trapping and stabilize the formation of I_3^-. Ultimately, this finding may have relevance also in 3D perovskites, where octahedral distortions may be finely tuned to modifying the tendency to undergo charge trapping. Further work is to be conducted in this direction.

In summary, we showed that geometrical distortions of the perovskite lattice closely affect its defectivity and corresponding charge relaxation dynamics, exemplified by the evidence of V_F centers formation in (EDBE)PbI_4. Our findings stress the importance of structural engineering in hybrid perovskites to achieve full control over the material properties, with high relevance for photovoltaic and light emission applications.

ASSOCIATED CONTENT

Supporting Information

Experimental and computational details, perovskite distortion parameters. This material is available free of charge via the Internet at http://pubs.acs.org.

AUTHOR INFORMATION

Corresponding Author

*Annamaria.Petrozza@iit.it; filippo@thch.unipg.it

Notes

The authors declare no competing financial interests.

ACKNOWLEDGMENT

We acknowledge the European 7th framework program under grant agreement no. 604032 of the MESO project, EU Horizon 2020 Research and Innovation Program under grant agreement no. 643238 (SYNCHRONICS), the Ministry of Education (MOE2013-T2-044) and the National Research Foundation (NRF-CRP14-2014-03) of Singapore.

REFERENCES

(1) Saparov, B.; Mitzi, D. B. *Chemical Reviews* **2016**, *116*, 4558.
(2) Cho, H.; Jeong, S.-H.; Park, M.-H.; Kim, Y.-H.; Wolf, C.; Lee, C.-L.; Heo, J. H.; Sadhanala, A.; Myoung, N.; Yoo, S.; Im, S. H.; Friend, R. H.; Lee, T.-W. *Science* **2015**, *350*, 1222.
(3) Kim, Y.-H.; Cho, H.; Lee, T.-W. *Proceedings of the National Academy of Sciences* **2016**, *113*, 11694.
(4) Tsai, H.; Nie, W.; Blancon, J.-C.; Stoumpos, C. C.; Asadpour, R.; Harutyunyan, B.; Neukirch, A. J.; Verduzco, R.; Crochet, J. J.; Tretiak, S.; Pedesseau, L.; Even, J.; Alam, M. A.; Gupta, G.; Lou, J.; Ajayan, P. M.; Bedzyk, M. J.; Kanatzidis, M. G.; Mohite, A. D. *Nature* **2016**, *536*, 312.
(5) Yuan, M.; Quan, L. N.; Comin, R.; Walters, G.; Sabatini, R.; Voznyy, O.; Hoogland, S.; Zhao, Y.; Beauregard, E. M.; Kanjanaboos, P.; Lu, Z.; Kim, D. H.; Sargent, E. H. *Nat Nano* **2016**, *11*, 872.
(6) Byun, J.; Cho, H.; Wolf, C.; Jang, M.; Sadhanala, A.; Friend, R. H.; Yang, H.; Lee, T.-W. *Advanced Materials* **2016**, *28*, 7515.
(7) Galkowski, K.; Mitioglu, A.; Miyata, A.; Plochocka, P.; Portugall, O.; Eperon, G. E.; Wang, J. T.-W.; Stergiopoulos, T.; Stranks, S. D.; Snaith, H. J.; Nicholas, R. J. *Energy & Environmental Science* **2016**, *9*, 962.
(8) Lanty, G.; Zhang, S.; Lauret, J. S.; Deleporte, E.; Audebert, P.; Bouchoule, S.; Lafosse, X.; Zuñiga-Pérez, J.; Semond, F.; Lagarde, D.; Médard, F.; Leymarie, J. *Physical Review B* **2011**, *84*, 195449.
(9) Deschler, F.; Price, M.; Pathak, S.; Klintberg, L. E.; Jarausch, D.-D.; Higler, R.; Hüttner, S.; Leijtens, T.; Stranks, S. D.; Snaith, H. J.; Atatüre, M.; Phillips, R. T.; Friend, R. H. *The Journal of Physical Chemistry Letters* **2014**, *5*, 1421.
(10) Dohner, E. R.; Jaffe, A.; Bradshaw, L. R.; Karunadasa, H. I. *Journal of the American Chemical Society* **2014**, *136*, 13154.
(11) Dohner, E. R.; Hoke, E. T.; Karunadasa, H. I. *Journal of the American Chemical Society* **2014**, *136*, 1718.
(12) Li, Y. Y.; Lin, C. K.; Zheng, G. L.; Cheng, Z. Y.; You, H.; Wang, W. D.; Lin, J. *Chemistry of Materials* **2006**, *18*, 3463.
(13) Yangui, A.; Garrot, D.; Lauret, J. S.; Lusson, A.; Bouchez, G.; Deleporte, E.; Pillet, S.; Bendeif, E. E.; Castro, M.; Triki, S.; Abid, Y.; Boukheddaden, K. *The Journal of Physical Chemistry C* **2015**, *119*, 23638.
(14) Hu, T.; Smith, M. D.; Dohner, E. R.; Sher, M.-J.; Wu, X.; Trinh, M. T.; Fisher, A.; Corbett, J.; Zhu, X. Y.; Karunadasa, H. I.; Lindenberg, A. M. *The Journal of Physical Chemistry Letters* **2016**, *7*, 2258.
(15) Cortecchia, D.; Yin, J.; Bruno, A.; Lo, S.-Z. A.; Gurzadyan, G. G.; Mhaisalkar, S. G.; Brèdas, J.-L.; Soci, C. *arXiv:1603.01284v2* **2016**.
(16) Pelant, I.; Valenta, J. *Luminescence Spectroscopy of Semiconductors*; OUP Oxford, 2012.
(17) Herklotz, A.; Wong, A. T.; Meyer, T.; Biegalski, M. D.; Lee, H. N.; Ward, T. Z. *Scientific Reports* **2016**, *6*, 26491.
(18) Egger, D. A.; Rappe, A. M.; Kronik, L. *Accounts of Chemical Research* **2016**, *49*, 573.
(19) Billing, D. G.; Lemmerer, A. *Acta Crystallographica Section B* **2007**, *63*, 735.
(20) Quarti, C.; Grancini, G.; Mosconi, E.; Bruno, P.; Ball, J. M.; Lee, M. M.; Snaith, H. J.; Petrozza, A.; Angelis, F. D. *The Journal of Physical Chemistry Letters* **2014**, *5*, 279.
(21) Brivio, F.; Frost, J. M.; Skelton, J. M.; Jackson, A. J.; Weber, O. J.; Weller, M. T.; Goñi, A. R.; Leguy, A. M. A.; Barnes, P. R. F.; Walsh, A. *Physical Review B* **2015**, *92*, 144308.
(22) Gottesman, R.; Gouda, L.; Kalanoor, B. S.; Haltzi, E.; Tirosh, S.; Rosh-Hodesh, E.; Tischler, Y.; Zaban, A.; Quarti, C.; Mosconi, E.; De Angelis, F. *The Journal of Physical Chemistry Letters* **2015**, *6*, 2332.
(23) Pérez-Osorio, M. A.; Milot, R. L.; Filip, M. R.; Patel, J. B.; Herz, L. M.; Johnston, M. B.; Giustino, F. *The Journal of Physical Chemistry C* **2015**, *119*, 25703.
(24) Ivanovska, T.; Quarti, C.; Grancini, G.; Petrozza, A.; De Angelis, F.; Milani, A.; Ruani, G. *ChemSusChem* **2016**, *9*, 2994.
(25) Teixeira-Dias, J. J. C.; de Carvalho, L. A. E. B.; da Costa, A. M. A.; Lampreia, I. M. S.; Barbosa, E. F. G. *Spectrochimica Acta Part A: Molecular Spectroscopy* **1986**, *42*, 589.
(26) Motti, S. G.; Gandini, M.; Barker, A. J.; Ball, J. M.; Srimath Kandada, A. R.; Petrozza, A. *ACS Energy Letters* **2016**, 726.
(27) Kong, W.; Ye, Z.; Qi, Z.; Zhang, B.; Wang, M.; Rahimi-Iman, A.; Wu, H. *Physical Chemistry Chemical Physics* **2015**, *17*, 16405.
(28) Neutzner, S.; Srimath Kandada, A. R.; Lanzani, G.; Petrozza, A. *Journal of Materials Chemistry C* **2016**, *4*, 4630.
(29) Wehrenfennig, C.; Liu, M.; Snaith, H. J.; Johnston, M. B.; Herz, L. M. *APL Mater.* **2014**, *2*, 081513.
(30) Thomas, N. *Acta Crystallographica Section B* **1989**, *45*, 337.
(31) Robinson, K.; Gibbs, G. V.; Ribbe, P. H. *Science* **1971**, *172*, 567.
(32) Mosconi, E.; Meggiolaro, D.; Snaith, H. J.; Stranks, S. D.; De Angelis, F. *Energy & Environmental Science* **2016**, *9*, 3180.

(33) Azpiroz, J. M.; Mosconi, E.; Bisquert, J.; De Angelis, F. *Energy & Environmental Science* **2015**, *8*, 2118.
(34) Du, M.-H. *The Journal of Physical Chemistry Letters* **2015**, *6*, 1461.
(35) Känzig, W. *Journal of Physics and Chemistry of Solids* **1960**, *17*, 80.
(36) Kao, C.-t.; Rowan, L. G.; Slifkin, L. M. *Physical Review B* **1990**, *42*, 3142.

TOC Figure:

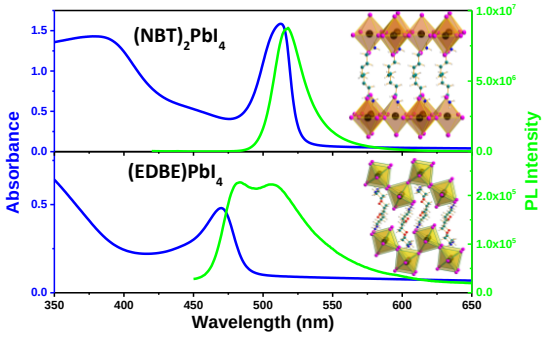

Supporting Information

Broadband Emission in Two-dimensional Hybrid Perovskites: the Role of Structural Deformation

Daniele Cortecchia[1,2], Stefanie Neutzner[2], Ajay Ram Srimath Kandada[2], Edoardo Mosconi[3,4], Daniele Meggiolaro[3,4],Filippo De Angelis[3,4*], Cesare Soci[5] and Annamaria Petrozza[2*]

1 Interdisciplinary Graduate School, Energy Research Institute @ NTU(ERI@N), Nanyang Technological University, Singapore 639798, Singapore.
2 Istituto Italiano de Tecnologia, Centre for Nano Science and Technology (CNST@PoliMi), Milan, 20133, Italy
3 Istituto CNR di Scienze e Tecnologie Molecolari, c/o Dipartimento di Chimica, Università di Perugia, Perugia, I-06123, Italy
4 CompuNet, Istituto Italiano di Tecnologia, Via Morego 30, 16163 Genova, Italy
5 Division of Physics and Applied Physics, School of Physical and Mathematical Sciences, Nanyang Technological University, Singapore 637371, Singapore.

*Annamaria.Petrozza@iit.it< filippo@thch.unipg.it

I. Materials and methods

The following inorganic precursors were used: lead(II) iodide (PbI2, 99.995%, Alfa Aesar), hydriodic acid HI (57% wt in water, distilled, stabilized, Sigma Aldrich), 2,2'-(ethylenedioxy)bis(ethylamine) (98%, Sigma Aldrich), n-butylammonium iodide (NBT)I (Dyesol), dimethyl sulfoxide DMSO (anhydrous, Sigma Aldrich), N,N-Dimethylformamide DMF (anhydrous, Sigma Aldrich).

Synthesis of (EDBE)I_2, where EDBE=2,2'-(ethylenedioxy)bis(ethylammonium): 1ml of 2,2'-(ethylenedioxy)bis(ethylamine) was dissolved in 10ml of ethanol end reacted with an excess of HI water solution. The acid was added dropwise to the amine solution under vigorous magnetic stirring and ice-bath cooling. After 4h of reaction, the solvent was removed by rotary evaporator, and the resulting yellow precipitate was washed by re-dissolving it in hot ethanol and precipitating with diethyl ether. The procedure was repeated several times (x6) until a white powder was obtained. This was finally dried in vacuum oven at 60 °C for 12h, and stored under N_2 inert atmosphere.

Perovskite thin film fabrication and characterization: the concentration of the precursor solutions was adjusted in order to obtain the desired film thickness. In the case of $(NBT)_2PbI_4$, a typical example

consists in the dissolution of 50.3 mg on (NBT)I and 57.6 mg of PbI_2 in 250 µl of DMSO (0.5 M solution). For (EDBE)PbI_4, 100.0 mg of (EDBE)I_2 and 115.2 mg of PbI_2 were dissolved in 500 µl of DMSO (0.5 M solution). Both the precursor solutions were spinned on the substrate at 4000 rpm, 30s, and the films annealed on the hotplate at 100° for 30 min. The resulting thin films were characterized through X-ray diffraction (XRD) using a BRUKER D8 ADVANCE with Bragg-Brentano geometry, Cu Kα radiation (α = 1.54,056 Å), step increment of 0.02° and 1 s of acquisition time.

Synthesis of perovskite single crystals: $(NBT)_2PbI_4$ and (EDBE)PbI_4 crystals were obtained following previously reported procedures. Slow cooling technique was used for $(NBT)_2PbI_4$: 100.52 mg of (NBT)I (Dyesol) and 115.25 mg of PbI2 where dissolved in 1.2 ml of hot concentrate HI water solution (100 °C). The solution was then slowly cooled (2 °C/h) at room temperature, and then left in refrigerator (2 °C) for one week. During this time, few orange perovskite crystals formed on the bottom of the vial. (EDBE)PbI_4 was synthetized by vapor diffusion method: 33.5 mg of 'home-made' (EDBE)I_2 and 26.5 mg of PbI_2 were dissolved in concentrated HI water solution (3 ml). The solution was left under diffusion of diethyl ether vapors for one week, causing the slow precipitation of small yellow crystals.

Optical characterization: steady state absorption spectra were measured on perovskite thin films using a UV/VIS/NIR spectrophotometer Lambda 1050, Perkin Elmer, while the photoluminescence emission spectra were measured with a NanoLog (Horiba Jobin Yvon). For the power dependent photoluminescence measurements the excitation source consists of a mode-locked Ti:sapphire oscillator (Coherent Micra) in conjunction with a regenerative amplifier (Coherent RegA 900), delivering 50 fs pulses at 800 nm central wavelength with 250 kHz repetition rate. The pump pulses were generated by frequency doubling the fundamental in a BBO crystal, focused with a 500 mm lens and arrived at an angle of approximately 45° to the sample surface. The photoluminescence was collected from the front by focusing into a fiber coupled spectrometer (Ocean Optics Maya pro 2000). A 450 nm long-pass filter was used in front of the spectrometer to prevent saturation by the scattered pump light. To derive the relative PLQY at each excitation density, the spectrally integrated photoluminescence signal was divided by the respective pump power. All PL measurements were carried out in vacuum to prevent sample degradation due to moisture and oxygen.

Raman characterization: the measurements were performed on perovskite single crystals and powders of the organic precursors. The Raman spectra of the materials were recorded in the range of 50-2000 cm^{-1} with a micro Raman confocal microscope (inVia Raman Microscope Renishaw, 10 x objective, 785 nm excitation wavelength). All measurements were carried out in air.

Computational methods: DFT calculations within periodic boundary conditions have been performed with planewave/pseudopotential formalism, as implemented in the PWSCF package of Quantum-Espresso.[1] For the geometry optimization we used PBE exchange-correlation functional[2] along with ultrasoft,[3] scalar relativistic pseudopotentials for all the atoms, by using the experimental cell parameters as found from XRD measurements. The cutoffs for the wave function and the electronic density expansions were set to 25 Ry and 200 Ry cutoffs, respectively.

We evaluated the electronic and optical properties of the (EDBE)PbI_4 system at the equilibrium structure found at the PBE level and by using the hybrid PBE0 functional[4] (α=0.30) including spin-orbit coupling. Norm conserving pseudo potentials have been used with wave function and electronic density cutoffs of 40 Ry and 160 Ry, respectively.

II. Compositional and morphological characterization of perovskite thin films.

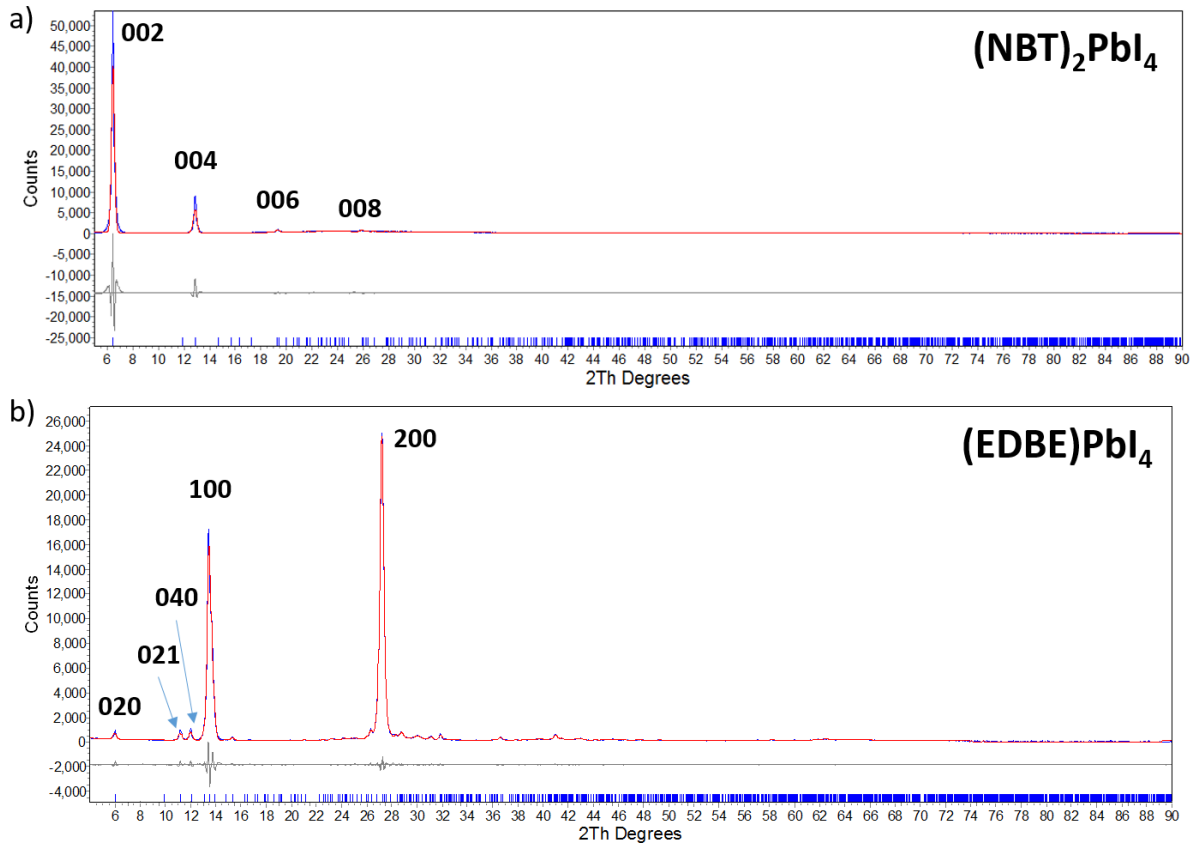

Figure S1. Perovskite thin film X-ray diffraction (XRD). Experimental (blue) and calculated (red) diffraction pattern by Pawley fitting. The grey line is the difference between the observed and experimental pattern, while the blue marks indicate the reflections expected for the corresponding perovskite phase. a) $(NBT)_2PbI_4$, the diffraction pattern is consistent with the expected crystal structure having orthorhombic crystal system, space group *Pbca*, and lattice parameters a = 8.8854 Å, b = 8.6249 Å c = 27.4588 Å. The film shows a strong preferential orientation towards the <*00l*> direction. b) $(EDBE)PbI_4$, the diffraction pattern is consistent with the expected crystal structure having monoclinic crystal system, space group *P21/c*, and lattice parameters a = 6.5459 Å, b = 29.3190 Å, c = 9.3356 Å, b= 92.46°. The film shows a strong preferential orientation towards the <*h0o*> direction.

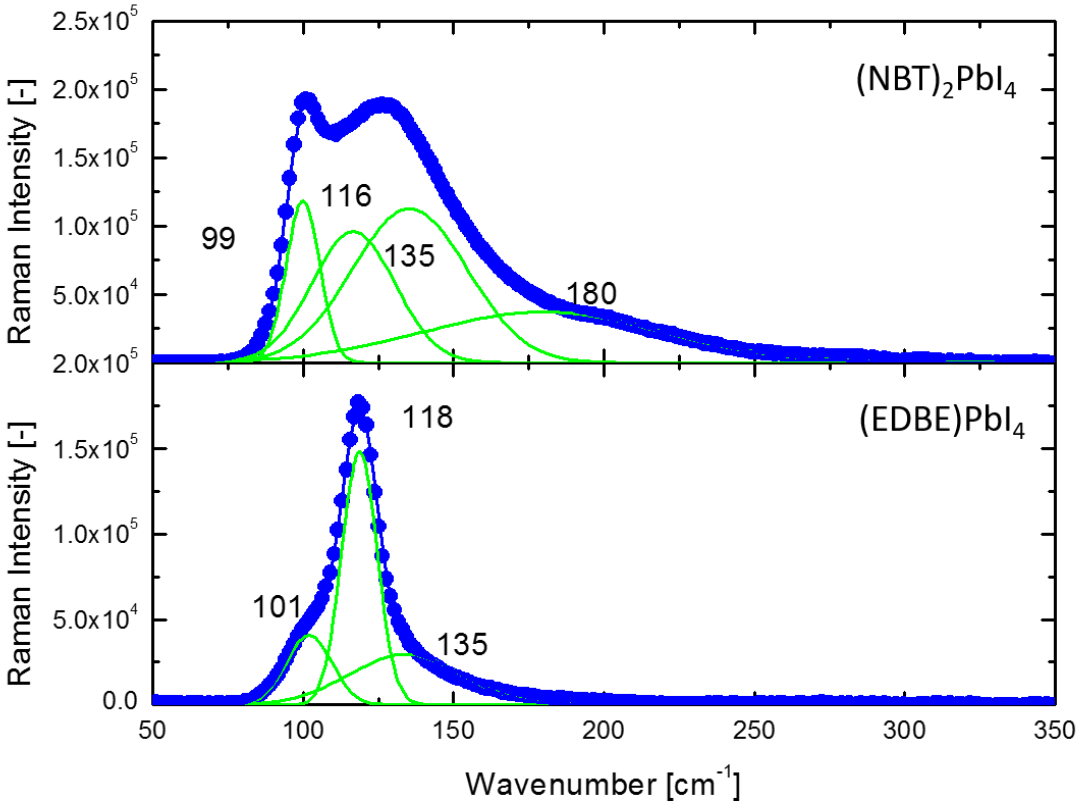

Figure S2. Raman spectra measured on perovskite films spin-coated on intrinsic silicon substrates: a) $(NBT)_2PbI_4$ and b) $(EDBE)PbI_4$. The low-frequency modes are consistent with those measured on perovskite single crystals.

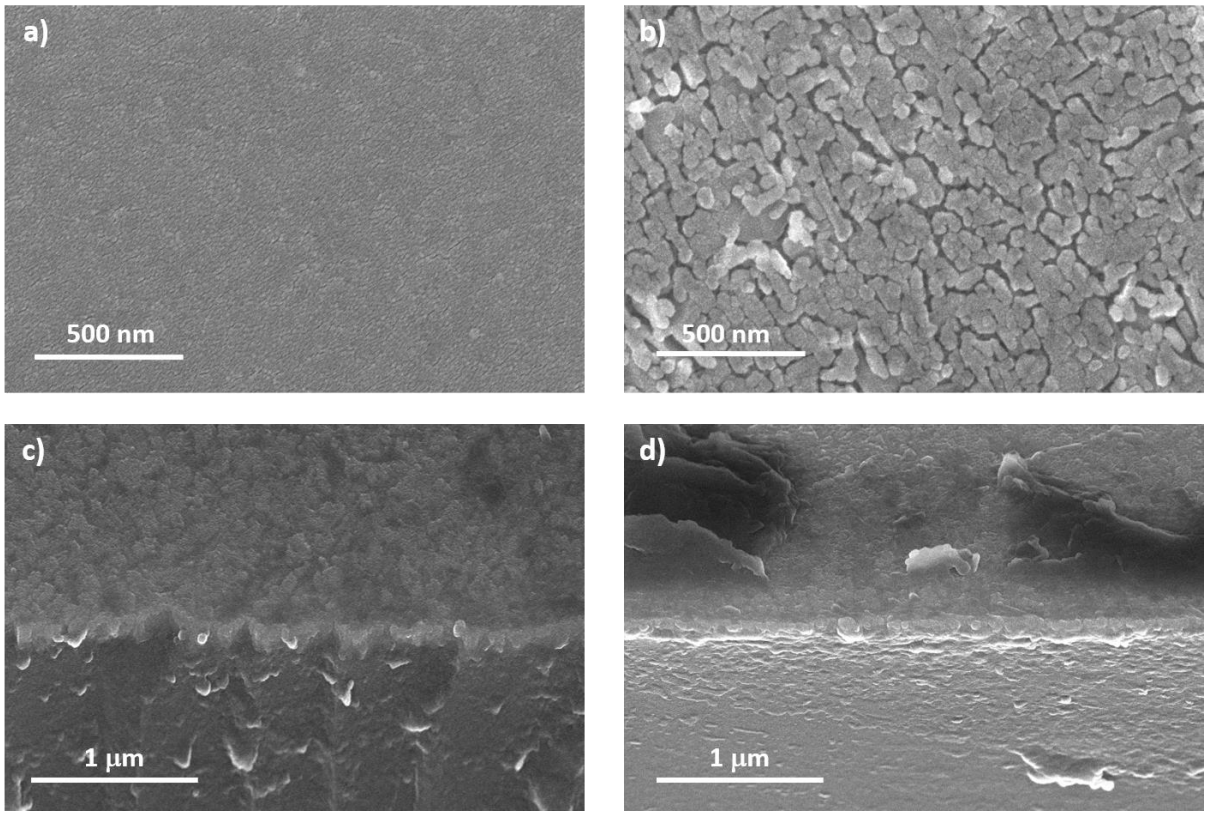

Figure S3. Scanning electron microscope (SEM) characterization of perovskite thin films spin-coated on ITO glass from 0.25M perovskite solutions in DMSO. Top view images of a) $(EDBE)PbI_4$ and b) $(NBT)_2PbI_4$ (scale bar = 500 nm). While $(EDBE)PbI_4$ forms an extremely smooth and compact film made of small perovskite grains, the NBT ligand promotes the growth of bigger crystals which do not form a perfectly compact film. The cross-section images show a similar thickness of about 100 nm for both the perovskites c) $(EDBE)PbI_4$ and d) $(NBT)_2PbI_4$ (scale bar = 1 μm).

III. Thickness dependence of (EDBE)PbI_4 photoluminescence.

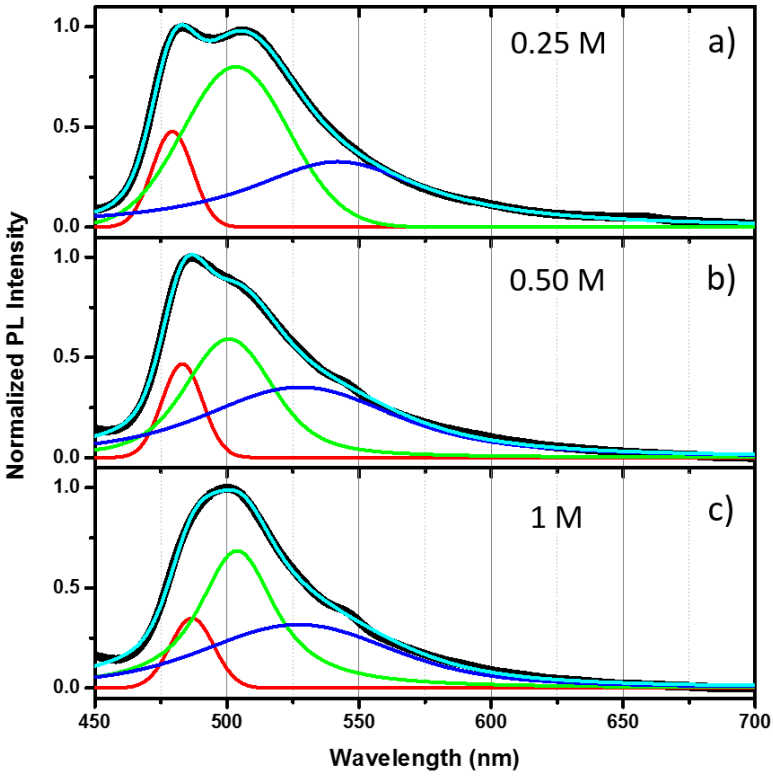

Figure S4. Thickness dependence of (EDBE)PbI_4 photoluminescence spectrum (excitation at λ_{exc} = 400 nm) and analysis by principle component fitting: a) thickness = 500±33 nm, b) thickness = 227±26 nm, b) thickness = 86±8 nm, achieved by modifying the concentration of the precursor solution from 0.25M to 1M. The excitonic component of the luminescence (red line) is better resolved in the emission spectrum when film thickness is <500 nm.

IV. Power-dependent photoluminescence measurements

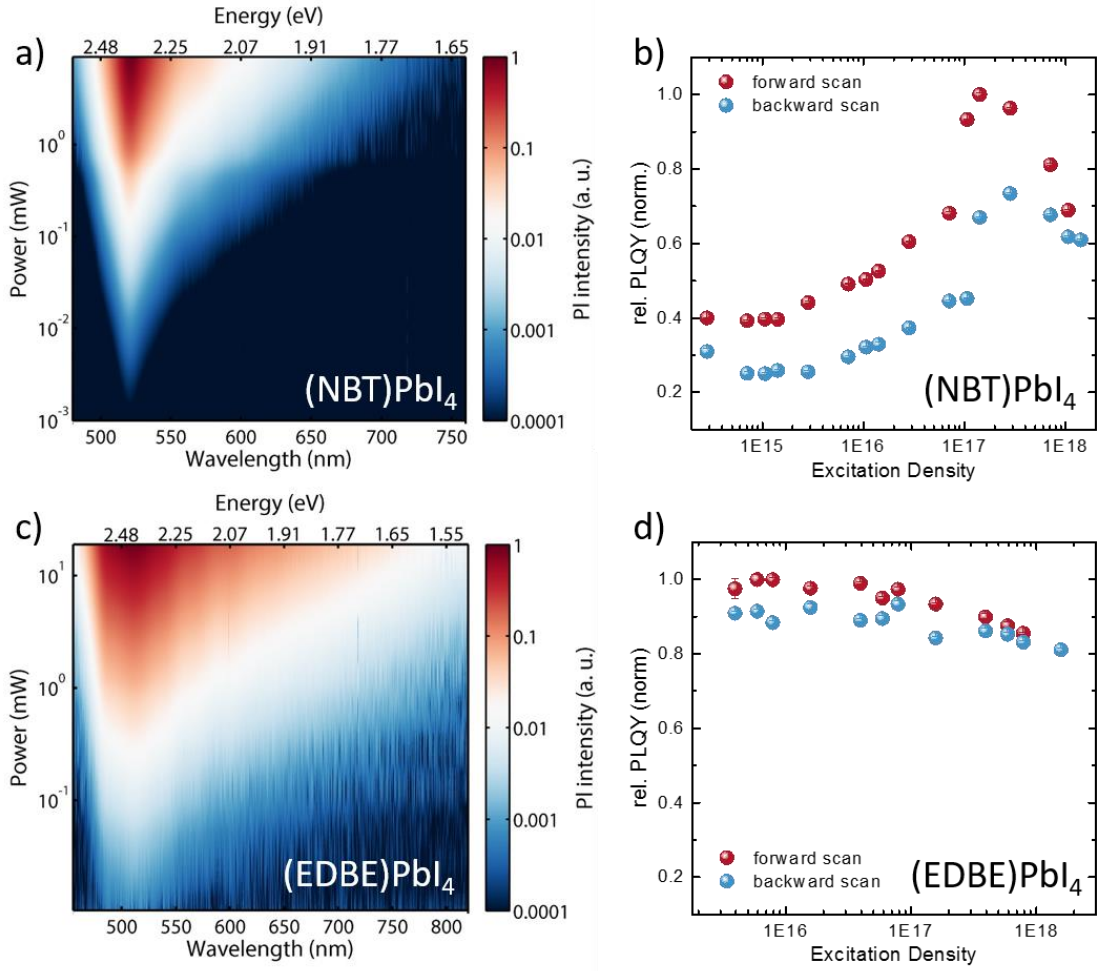

Figure S5. Photoluminescence (PL) power dependence and relative photoluminescence quantum yield (PLQY) against excitation density for a,b) $(NBT)_2PbI_4$ and c,d) $(EDBE)PbI_4$. The relative PLQY trends point out the different origin of the photoluminescence in the two systems. In the case of $(NBT)_2PbI_4$, the increasing trend of the relative PLQY with excitation density is consistent with a trap limited recombination mechanism, while non radiative Auger recombination is responsible for the PL quenching at high excitation densities (b). On the other hand, the monotonic decrease of relative PLQY of the P2 band in $(EDBE)PbI_4$ indicates that the photoluminescence in this material stems from intra-band trap states saturated at high density (d).

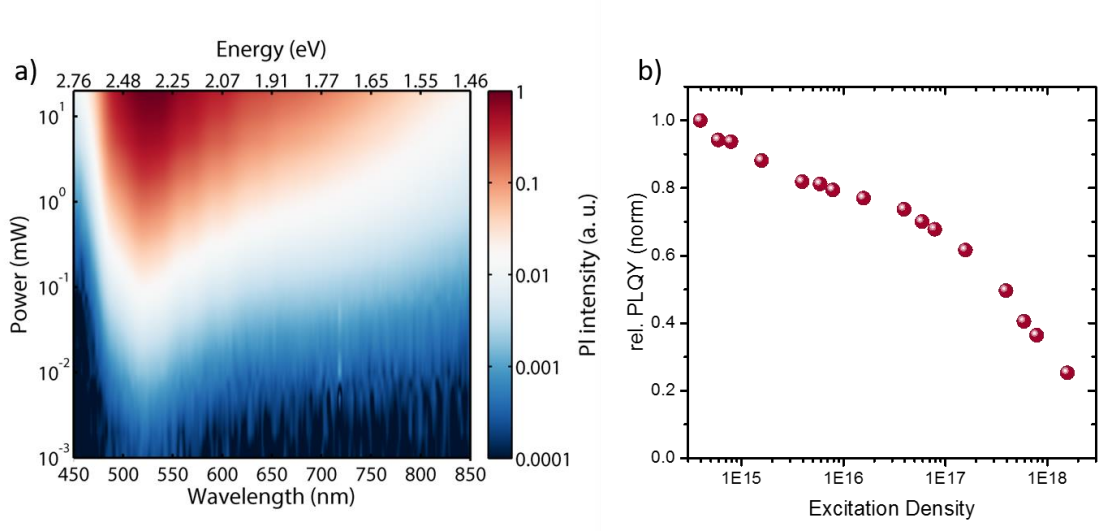

Figure S6. a) Photoluminescence (PL) power dependence and b) relative photoluminescence quantum yield (PLQY) against excitation density measured on (EDBE)PbI_4 single crystals.

V. Analysis of structural distortions in two-dimensional perovskites

Structural distortion parameters have been calculated (using VESTA) from the published crystallographic data of all the reported broadband emitting perovskites and a selected group of narrowband emitting perovskites (Figure 7, Table 1 and 2): (API)$PbBr_4$,[5] (AETU)$PbBr_4$,[6] (N-MEDA)$PbBr_4$,[7] (EDBE)$PbBr_4$,[8] (EDBE)PbI_4,[8] (EDBE)$PbCl_4$,[8] $(CEA)_2PbBr_4$,[9] $(NBT)_2PbI_4$,[10] (NMPDA)$PbBr_4$,[7] $(PEA)_2PbCl_4$,[11] $(PEA)_2PbBr_4$,[11] (MA)$PbBr_3$,[12] (MA)PbI_3.[13] The distortion of the inorganic building block, the octahedra PbX_6, was evaluated by mean of the following parameters:

Bond-length distortion[14]: $\Delta_{oct} = \frac{1}{6}\sum_{i=1}^{6}[(d_i - d_m)/d_m]^2$

Octahedral elongation[15,16]: $\lambda_{oct} = \frac{1}{6}\sum_{i=1}^{6}(d_i/d_0)^2$

where d_i is the Pb-X bond length, d_m is the average bond length and d_o is the center-to-vertex distance of a regular polyhedron of the same volume. Δ_{oct} and λ_{oct} are dimensionless, and give a quantitative measure of polyhedral disortion independently of the polyhedron effective size.

Halide Distance Deviation[14]: $DI(X-X) = [\sum_{i=1}^{12}|(X-X)_i - (X-X)_m|]/12 * (X-X)_m$

where $(X\text{-}X)_i$ is the distance between adjacent halides corresponding to the octahedral edges length, and $(X\text{-}X)_m$ is the average halide distance.

Octahedral angle variance[14-17]: $\boldsymbol{\sigma^2_{oct} = \frac{1}{11}\sum_{i=1}^{12}(\alpha_i - 90)^2}$

where a_i represents the individual X-Pb-X angle.

Volume discrepancy[18]: $\boldsymbol{v(\%) = (V_m - V_r) * 100/V_m}$

where *Vr* is the volume of the coordination octahedral PbX_6 and V_m is the volume of the corresponding ideal octahedral having edges of lengths equal to $(X\text{-}X)_m$. The volume discrepancy measures how much the ligand atoms are regularly distributed, independently on the position of the central atom (Pb, in this case) within the octahedron.

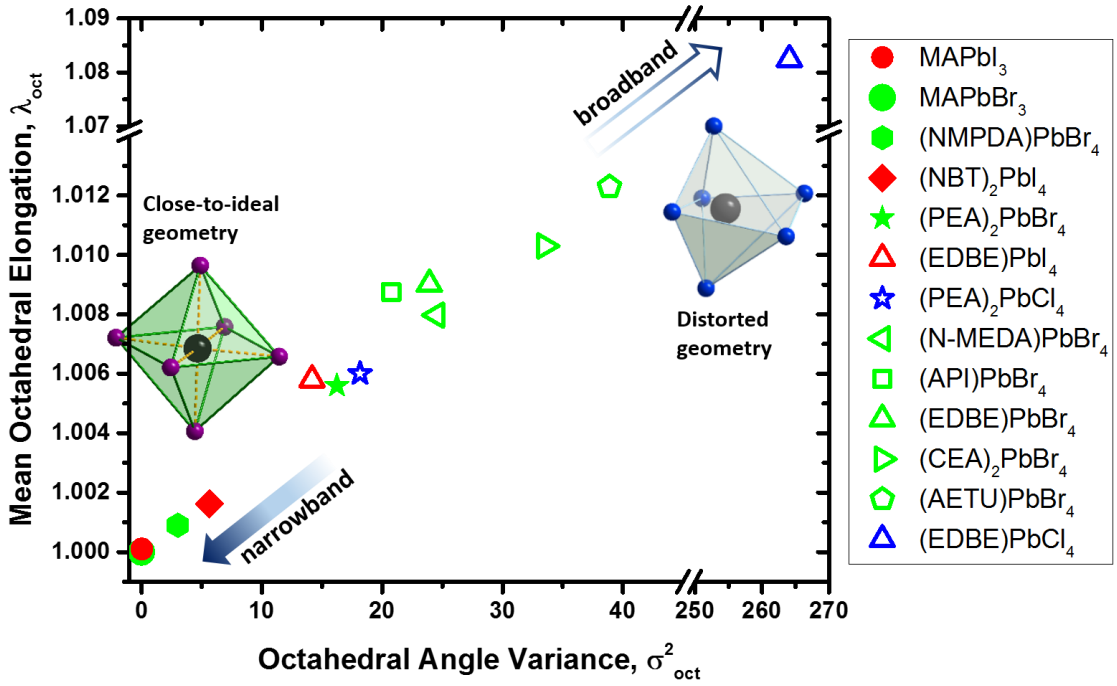

Figure S7. Mean octahedral elongation λ_{oct} against octahedral angle variance σ^2_{oct}. Color code: red = iodide-based perovskites, green = bromide-based perovskites, blue = chloride-based perovskites. Markers with solid interior indicates narrowband emitting perovskites, while open interior denotes perovskites characterized by broadened photoluminescence. λ_{oct} and σ^2_{oct} have been introduced by K. Robinson *et al*[15] for the quantitative analysis of structural distortions in a variety of mineral groups. Such parameters allow the direct evaluation of the distortion of coordination polyhedra within a crystal structure, and is much more specific than the evaluation based on the unit cell of the material. From this plot, a direct comparison between perovskites based on the same halide indicates that increased structural strain is correlated to the emergence of broadened photoluminescence in hybrid perovskites.

Table S1. Distortion parameters calculated for broadband emitting hybrid perovskites.

Organic Cation	Name and Abbreviation	Perovskite Fromula	Perovskite Type and Orientation	DI(X-X)	$\Delta_{oct}x10^3$	ν(%)	λ_{oct}	σ_{oct}^2	Ref.
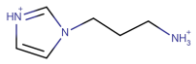	N-(3-aminopropyl)imidazole [API]	**$(API)PbBr_4$**	2D - <110>	**0.029**	**2.60**	**0.67**	**1.0088**	**20.8**	**5**
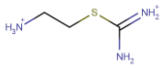	2-(aminoethyl)isothiourea [AETU]	**$(AETU)PbBr_4$**	2D - <110>	**0.047**	**0.97**	**1.59**	**1.0123**	**38.9**	**6**
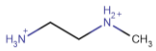	N1-methylethane-1,2-diammonium [N-MEDA]	**$(N\text{-}MEDA)PbBr_4$**	2D - <110>	**0.040**	**0.82**	**0.79**	**1.0080**	**24.5**	**7**
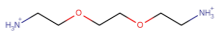	2,2'-(ethylenedioxy)bis(ethylammonium) [EDBE]	**$(EDBE)PbBr_4$**	2D - <110>	**0.044**	**2.40**	**0.96**	**1.0090**	**23.9**	**8**
		(EDBE)PbI4	2D - <110>	**0.030**	**1.90**	**0.50**	**1.0058**	**14.2**	**8**
		$(EDBE)PbCl_4$	2D - <100>	**0.088**	**0.056**	**13.02**	**1.0824**	**264.2**	**8**
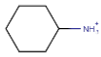	cyclohexylammonium [CEA]	**$(CEA)_2PbBr_4$**	2D - <100>	**0.051**	**0.6**	**0.47**	**1.0103**	**33.5**	**9**
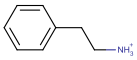	phenethylammonium [PEA]	**$(PEA)_2PbCl_4$**	2D - <100>	**0.026**	**0.781**	**0.20**	**1.0060**	**18.7**	**11**

Table S2. Distortion parameters calculated for narrowband emitting hybrid perovskites.

Organic Cation	Name and Abbreviation	Perovskite Formula	Perovskite Type and Orientation	DI(X-X)	$\Delta_{oct}x10^3$	ν(%)	λ_{oct}	σ_{oct}^2	Ref.
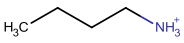	n-butylammonium [BA]	**$(NBT)_2PbI_4$**	2D - <100>	**0.017**	**0.011**	**0.18**	**1.0016**	**5.6**	**10**
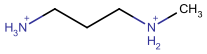	N1-methylpropane-1,3-diammonium [N-MPDA]	**$(NMPDA)PbBr_4$**	2D - <100>	**0.014**	**0.050**	**0.13**	**1.0009**	**3.0**	**7**
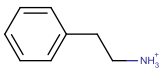	phenethylammonium [PEA]	**$(PEA)_2PbBr_4$**	2D - <100>	**0.020**	**0.989**	**0.19**	**1.0056**	**16.5**	**11**
	methylammonium [MA]	**$(MA)PbBr_3$**	3D - <100>	**0.000**	**0.000**	**0.00**	**1.0000**	**0.00**	**12**
		$(MA)PbI_3$	3D - <100>	**0.005**	**0.0005**	**0.04**	**1.0001**	**0.03**	**13**

VI. Computational Details

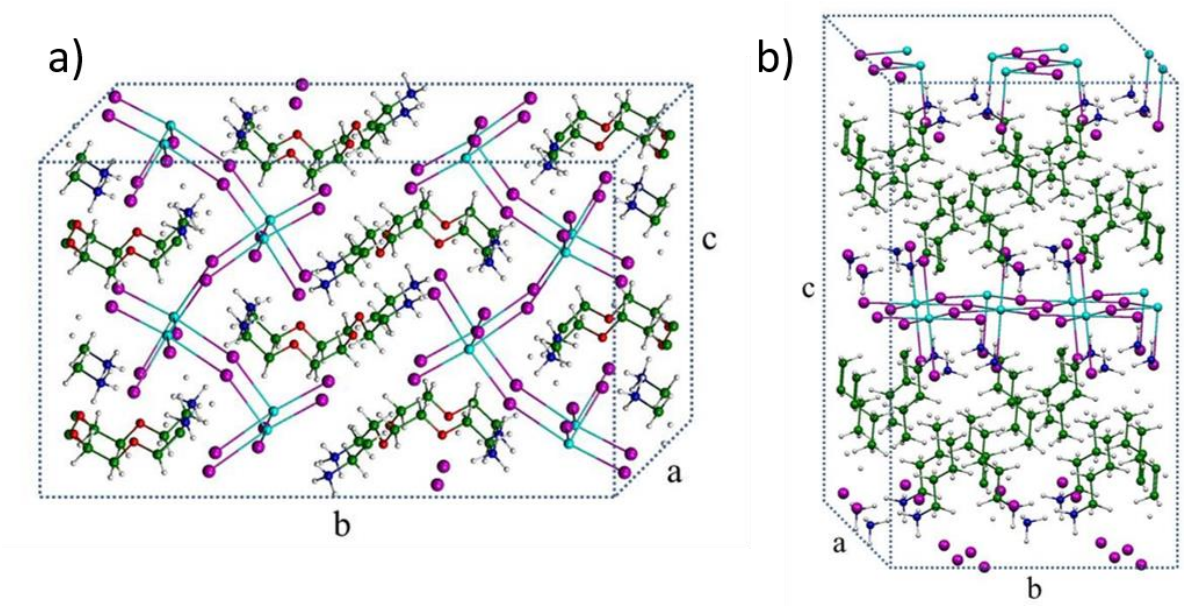

Figure S8. Structural relaxation at Γ on a supercell at scalar relativistic GGA level, 25/200 Ry using the experimental cell parameters. Symmetry was disabled. a) Optimized geometry of (EDBE)PbI_4. Experimental cell parameter from CIF[8]: a=6.49405 Å, b=29.4612 Å, c=9.26667 Å, β=91.777°; space group = Monoclinic P21/c; model = 2x1x2 supercell at Γ. b) Optimized geometry of $(NBT)_2PbI_4$. Experimental cell Parameters from CIF[10]: a=8.87641 Å, b=8.69251 Å, c=27.60145 Å, space group = orthorhombic Pbca, model = 2x2x1 supercell at Γ.

Table S3. Calculated Band Gap (eV) for the investigate species and relative defective materials at the scalar relativist PBE GGA level of theory.

		EDBE		NBT	
		Rel. En.	Gap	Rel. En.	Gap
Perf. Cryst.		-	2.21	-	2.04
VAC Pb*	-	-	1.40	-	1.25
VAC I	ap. External	**0.00**	**1.91**	**0.00**	**1.69**
	ap. Inner	0.31	1.91	-	-
	eq.	0.26	1.42	0.04	1.48
INT I	ap. External	0.26	1.74	0.04	1.49
	ap. Inner	**0.00**	**1.84**	-	-
	eq.	0.21	1.65	**0.00**	**1.69**

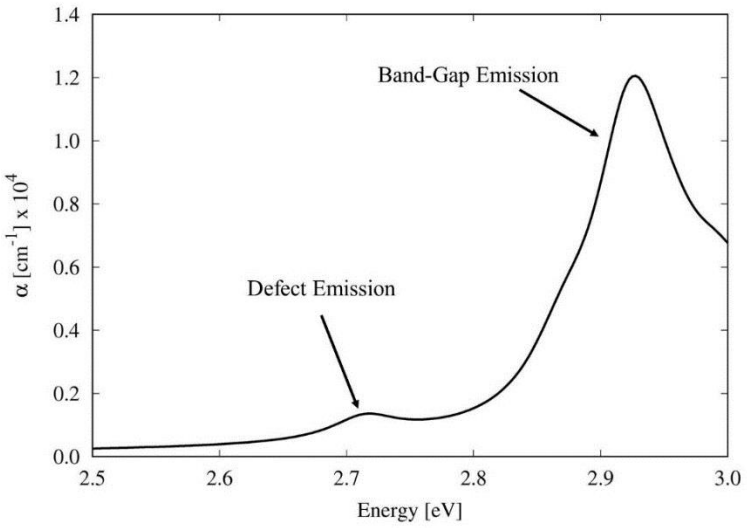

Figure S9. Calculated absorption spectrum (RPA) of the neutral (EDBE)PbI_4 with the lead vacancy.

References

(1) Paolo, G.; Stefano, B.; Nicola, B.; Matteo, C.; Roberto, C.; Carlo, C.; Davide, C.; Guido, L. C.; Matteo, C.; Ismaila, D.; Andrea Dal, C.; Stefano de, G.; Stefano, F.; Guido, F.; Ralph, G.; Uwe, G.; Christos, G.; Anton, K.; Michele, L.; Layla, M.-S.; Nicola, M.; Francesco, M.; Riccardo, M.; Stefano, P.; Alfredo, P.; Lorenzo, P.; Carlo, S.; Sandro, S.; Gabriele, S.; Ari, P. S.; Alexander, S.; Paolo, U.; Renata, M. W. *Journal of Physics: Condensed Matter* **2009**, *21*, 395502.
(2) Perdew, J. P.; Burke, K.; Ernzerhof, M. *Physical Review Letters* **1996**, *77*, 3865.
(3) Vanderbilt, D. *Physical Review B* **1990**, *41*, 7892.
(4) Perdew, J. P.; Ernzerhof, M.; Burke, K. *The Journal of Chemical Physics* **1996**, *105*, 9982.
(5) Li, Y. Y.; Lin, C. K.; Zheng, G. L.; Cheng, Z. Y.; You, H.; Wang, W. D.; Lin, J. *Chemistry of Materials* **2006**, *18*, 3463.
(6) Li, Y.; Zheng, G.; Lin, J. *European Journal of Inorganic Chemistry* **2008**, *2008*, 1689.
(7) Dohner, E. R.; Hoke, E. T.; Karunadasa, H. I. *Journal of the American Chemical Society* **2014**, *136*, 1718.
(8) Dohner, E. R.; Jaffe, A.; Bradshaw, L. R.; Karunadasa, H. I. *Journal of the American Chemical Society* **2014**, *136*, 13154.
(9) Yangui, A.; Garrot, D.; Lauret, J. S.; Lusson, A.; Bouchez, G.; Deleporte, E.; Pillet, S.; Bendeif, E. E.; Castro, M.; Triki, S.; Abid, Y.; Boukheddaden, K. *The Journal of Physical Chemistry C* **2015**, *119*, 23638.
(10) Billing, D. G.; Lemmerer, A. *Acta Crystallographica Section B* **2007**, *63*, 735.
(11) Mitzi, D. B. *Journal of Solid State Chemistry* **1999**, *145*, 694.
(12) Jaffe, A.; Lin, Y.; Beavers, C. M.; Voss, J.; Mao, W. L.; Karunadasa, H. I. *ACS Central Science* **2016**, *2*, 201.
(13) Stoumpos, C. C.; Malliakas, C. D.; Kanatzidis, M. G. *Inorganic Chemistry* **2013**, *52*, 9019.
(14) Ertl, A.; Hughes, J. M.; Pertlik, F.; Jr., F. F. F.; Wright, S. E.; Brandstatter, F.; Marler, B. *Can Mineral* **2002**, *40*, 153.

(15) Robinson, K.; Gibbs, G. V.; Ribbe, P. H. *Science* **1971**, *172*, 567.
(16) Thomas, N. *Acta Crystallographica Section B* **1989**, *45*, 337.
(17) Fleet, M. E. *Mineralogical Magazine* **1976**, *40*, 531.
(18) Makovicky, E.; Balic-Zunic, T. *Acta Crystallographica Section B* **1998**, *54*, 766.